

32 **Abstract**

33

34 Mercury was measured onboard the IAGOS-CARIBIC passenger aircraft since May 2005
35 until February 2016 during nearly monthly sequences of mostly four intercontinental
36 flights from Germany to destinations in North and South America, Africa, and South and
37 East Asia. Most of these mercury data were obtained using an internal default signal
38 integration procedure of the Tekran instrument but since April 2014 more precise and
39 accurate data were obtained using post-flight manual integration of the instrument raw
40 signal. In this paper we use the latter data.

41

42 Elevated upper tropospheric total mercury (TM) concentrations due to large scale biomass
43 burning were observed in the upper troposphere (UT) at the equator and southern latitudes
44 during the flights to Latin America and South Africa in boreal autumn (SON) and boreal
45 winter (DJF). TM concentrations in the lowermost stratosphere (LMS) decrease with
46 altitude above the thermal tropopause but the gradient is less steep than reported before.
47 Seasonal variation of the vertical TM distribution in the UT and LMS is similar to that of
48 other trace gases with surface sources and stratospheric sinks. Using speciation
49 experiments, we show that nearly identical TM and gaseous elementary mercury (GEM)
50 concentrations exist at and below the tropopause. Above the thermal tropopause GEM
51 concentrations are almost always smaller than those of TM and the TM – GEM (i.e. Hg^{2+})
52 difference increases up to ~40% of TM at ~2 km and more above the thermal tropopause.
53 Correlations with N_2O as a reference tracer suggest stratospheric lifetimes of 72 ± 37 and
54 74 ± 27 yr for TM and GEM, respectively, comparable to the stratospheric lifetime of COS.
55 This coincidence, combined with pieces of evidence from us and other researchers,
56 corroborates the hypothesis that Hg^{2+} formed by oxidation in the stratosphere attaches to
57 sulfate particles formed mainly by oxidation of COS and is removed with them from the
58 stratosphere by air mass exchange, gravitational sedimentation, and cloud scavenging
59 processes.

60

61 **1 Introduction**

62

63 Mercury is ~~a heavy metal~~an element whose high vapor pressure leads to significant
64 emissions into the atmosphere. ~~Moreover, due to its slow rate~~Measurements of oxidation
65 ~~and low solubility in water it can be transported~~atmospheric mercury show a relatively
66 ~~even distribution~~ over ~~long distances~~the globe (Sprovieri et al., 2010) with concentrations
67 ~~varying mostly between 1 – 2 ng m⁻³ in remote areas~~. After oxidation to less volatile and
68 more soluble compounds, mercury is ~~thus deposited in remote areas~~and becomes
69 ~~bioavailable~~. Its conversion to the highly neurotoxic methyl mercury which
70 bioaccumulates in the aquatic nutritional chain to concentrations dangerous for humans
71 and animals has motivated intensive research on the biogeochemical cycle of mercury (e.g.
72 Mergler et al., 2007; Scheuhammer et al., 2007; Lindberg et al., 2007, AMAP/UNEP, 2013
73 and references therein).

74

75 Despite decades of research, the atmospheric mercury cycle is still not well understood
76 (Lin et al., 2006; Lindberg et al., 2007, Ariya et al., 2015). Several mechanisms of
77 elemental mercury oxidation in the gas phase have been proposed (Selin et al., 2007;
78 Holmes et al., 2010; Dibble et al., 2012; Horowitz et al., 2017, Travnikov et al., 2017) but
79 their relative importance is still unknown (Lin et al., 2006; Travnikov et al., 2017). Neither
80 have the oxidation products been unequivocally identified so far because of the lack of
81 speciation techniques for individual mercury compounds (Gustin et al., 2015; Ariya et al.,
82 2015). In addition, attempts to constrain the atmospheric mercury cycle using different
83 models had to rely almost exclusively on measurements at the surface in the northern
84 hemisphere, which undermined these efforts. Measurements of mercury distribution in the
85 troposphere and stratosphere by research aircraft are expensive and thus usually limited to
86 short-term campaigns covering small regions of the globe (Ebinghaus and Slemr, 2000;
87 Friedli et al., 2001, 2003a and 2004; Banic et al., 2003; Ebinghaus et al., 2007; Radke et
88 al., 2007, Talbot et al., 2007a and b, Swartzendruber et al., 2008; Slemr et al., 2009; Lyman
89 and Jaffe, 2012; Brooks et al., 2014, Slemr et al., 2014; Ambrose et al., 2015; Gratz et al.,
90 2015; Weigelt et al., 2016a and b). These measurements have so far provided information
91 about the emissions of mercury from biomass burning (Friedli et al., 2001, 2003a and b;
92 Ebinghaus et al., 2007) and from industrial sources (Friedli et al., 2004; Talbot et al.,
93 2007b; Swartzendruber et al., 2008, Slemr, et al., 2014; Ambrose et al., 2015; Weigelt et

94 al., 2016b), with sometimes ~~conflicting~~[differing](#) information about the vertical distribution
95 of mercury (Ebinghaus and Slemr, 2000; Radke et al., 2007; Talbot et al., 2007a and b;
96 Slemr et al., 2009; Lyman and Jaffe, 2012; Brooks et al., 2014; Weigelt et al., 2016a; Bieser
97 et al., 2017). In addition, a pronounced depletion of elemental mercury in air masses
98 influenced by the stratosphere has been reported (Ebinghaus et al., 2007; Radke et al.,
99 2007; Talbot et al., 2007a and b, Swartzendruber et al., 2008, Slemr et al., 2009; Lyman
100 and Jaffe., 2012). Because of temporal and spatial limitations resulting from the costs of
101 research aircraft hardly any information on seasonal variation of mercury concentrations
102 in the upper troposphere (UT) and lowermost stratosphere (LMS) have been obtained so
103 far.

104

105 IAGOS-CARIBIC (*In-service Aircraft for a Global Observing System - Civil Aircraft for*
106 *Regular Investigation of the Atmosphere Based on an Instrumented Container*) project
107 offers a possibility of regular large scale sounding of trace gas distributions in the
108 ~~UT/LMS~~[UT/LMS](#) using an instrumented container flown onboard a passenger aircraft during
109 intercontinental flights (Brenninkmeijer et al., 2007, www.caribic-atmospheric.com).
110 From May 2005 until February 2016 mercury was measured with a modified Tekran
111 instrument in combination with a large suite of other trace gases and particles onboard the
112 CARIBIC aircraft (Brenninkmeijer et al., 2007, Slemr et al., 2009, 2014, 2016). The
113 mercury data collected during nearly monthly sequences of mostly four intercontinental
114 flights from Germany to destinations in North and South America, Africa, and East and
115 South Asia represent the largest mercury data set obtained in the UT and LMS so far. Most
116 mercury data were obtained using the Tekran internal default signal integration procedure
117 but since April 2014 we manually integrated the Tekran raw signal after the flights. The
118 post-flight integration of the raw signal substantially improved the detection limit and
119 precision of the mercury measurements and removed negative bias of the default
120 integration leading to occasional occurrence of zero concentrations in the data before April
121 2014 (Slemr et al., 2016; Ambrose, 2017). Raw signal data are available only since April
122 2014 and older data cannot be reintegrated. We use here the recent, smaller but higher
123 quality dataset, [in an attempt to figure out/unravel the fate/behavior](#) of mercury in the
124 ~~lowermost stratosphere~~[UT/LMS](#).

125

126 **2 Experimental**

127

128 The CARIBIC container (Brenninkmeijer et al., 2007; www.caribic-atmospheric.com)
129 onboard an Airbus 340-600 of Lufthansa holds automated analyzers for gaseous mercury,
130 CO, O₃, NO, NO_y, CO₂, CH₄, acetone, acetonitrile, water vapor (total, gaseous, isotope
131 composition), and fine aerosol particles (three counters for particles with lower threshold
132 diameters of 4 nm, 12 nm, and 18 nm, upper cut off about 2.0 μm), as well as an optical
133 particle size spectrometer (OPSS) for particles with diameters > 150 nm. In addition, whole
134 air and aerosol particle samples are taken in flight and subsequently analyzed for
135 greenhouse gases, halocarbons, hydrocarbons, and particle elemental composition. The
136 CARIBIC measurement container is usually deployed monthly during a sequence of four
137 intercontinental flights.

138

139 The air inlet system and the mercury instrument are described in detail by Brenninkmeijer
140 et al. (2007) and Slemr et al. (2016), respectively. Briefly, the trace gas inlet consists of a
141 trace gas diffuser tube with a flow of more than 2000 volume-l min⁻¹ from which ~80
142 volume-l min⁻¹ is taken at a right angle to a manifold which supplies the trace gas analyzers
143 in the container via a temperature controlled PFA lined supply line. The large air velocity
144 in the trace gas diffuser tube and perpendicular sampling at much smaller velocity
145 discriminate against particles larger than about one micrometer diameter (~50% aspiration
146 efficiency, Baron and Willeke, 2001). A modified Tekran instrument (Tekran-Analyzer
147 Model 2537 A, Tekran Inc., Toronto, Canada) samples 0.5 l (STP, i.e. 1013.25 hPa and
148 273.15 K) min⁻¹ of air from the supply line manifold (heated to 40°C) using the 4 mm ID
149 PFA tubing at about 30°C. The major modifications of the instrument were the addition of
150 a second pump supporting the internal Tekran pump and of a computer which
151 communicates with the container master computer and controls the automatic operation of
152 the instrument. For the period August 2014 until February 2016 a quartz wool scrubber
153 was installed in the instrument to filter out gaseous oxidized mercury (GOM).

154

155 To achieve an improved spatial resolution of ~ 75 km, the instrument was run with a
156 sampling time of only 5 min. Despite an additional pump the nominal flow of 0.5 l (STP)
157 min^{-1} could not be sustained at the highest flight levels. Limited air flow, the short sampling
158 time, and low concentrations resulted in only ~ 2 pg of mercury which is much smaller than
159 10 pg considered as minimum for bias-free internal default integration of the signal by the
160 Tekran instrument (Swartzendruber et al., 2009; Slemr et al., 2016; Ambrose, 2017). The
161 raw analyzer signals were thus processed post-flight using a manual integration procedure
162 described in detail by Slemr et al. (2016). The detection limit and precision with post-flight
163 processing is estimated to be ~ 0.05 ng m^{-3} . The instrument is calibrated after every second
164 flight sequence by comparison with a calibrated reference Tekran instrument in the
165 laboratory. All [mercury](#) concentrations are reported in ng Hg m^{-3} (STP).

166
167 As discussed in detail by Slemr et al. (2016) we can assume that our measurements
168 encompass gaseous elemental mercury (GEM), gaseous oxidized mercury (GOM), and
169 about 70% of particle bound mercury (PBM). Speciation experiments with soda lime and
170 KCl coated quartz sand as GOM scrubbers made during several flights demonstrated that
171 GOM passes through the CARIBIC sampling system. According to the extrapolation of
172 the reported GOM/PBM (GOM and PBM are both assumed to be Hg^{2+} , i.e. $\text{PBM} + \text{GOM}$
173 $= \text{Hg}^{2+}$) partitioning equilibria (Rutter and Schauer, 2007; Amos et al., 2012) from ambient
174 temperatures near ground to [about](#) -50°C around the tropopause, most of Hg^{2+} will be
175 attached to particles. Although the CARIBIC trace gas inlet is not optimized to collect
176 particles, we estimated that particles with diameter of < 0.5 μm will pass through it,
177 representing $\sim 70\%$ of the aerosol mass. Despite of significant PBM concentrations in the
178 stratosphere reported by Murphy et al. (1998, 2006), we were not able to detect mercury in
179 aerosol samples collected by the CARIBIC impactor sampler downstream of the inlet
180 optimized for quantitative particle sampling. Although not equipped with heaters, the air
181 carrying particles will warm up to $\sim +30^\circ$ on the way from the aerosol inlet to the impactor.
182 Our inability to detect mercury in particle samples thus suggests that Hg^{2+} on particles
183 evaporates when the air sample is heated to $\sim +30^\circ\text{C}$ in the inlet tubing and forms GOM.
184 In summary, we assume that our measurements are close to total mercury ($\text{TM} = \text{GEM} +$
185 $\text{Hg}^{2+} = \text{GEM} + \text{GOM} + \text{PBM}$) concentration and we refer to them as such.

186

187 In order to get information about the ~~GOM~~GEM fraction, sample air was passed through a
188 quartz wool scrubber of GOM (Lyman and Jaffe, 2012) during the outbound flights
189 between August 2014 and February 2016. ~~Quartz wool GOM~~The discussion of the use of
190 scrubbers are claimed not to be influenced by ozone (Ambrose and denuders has been going
191 now for more than a decade, so far without any firm conclusion on a reliable and accurate
192 method of separating GEM, GOM, and PBM (Gustin et al., 2013 and 2015) but can release
193 GOM2014). As described in humid air. Thus high UT/LMS ozone levels pose no problem
194 and humidity effects are likely small or absentSupplementary Information the quartz wool
195 scrubbers were operated within the range of parameters tested by Lyman and Jaffe (2012)
196 and we thus expect our data to be of comparable quality to theirs. The data collected with
197 quartz wool scrubber are referred here as GEM. However, during half of the flights with
198 quartz wool scrubber GEM concentrations were significantly higher than those of TM
199 during the return flight at the beginning of the flight and the difference decreased during
200 the flights indicating contamination ~~of unknown origin~~. We found that the contamination
201 started to occur after the change of the personnel operating the instrument and thus
202 attributed it to this change. These data were eliminated from the data set. We note that the
203 tracks and altitudes of the outbound and return flights differ sometimes substantially,
204 especially in the case of the flights to North America (the flight tracks from Germany to
205 North America tend to be substantially further north than those of the return flights). The
206 TM and GEM data are thus not directly comparable even if they were measured on the
207 same day.

208

209 The data reported here were obtained during flights between April 2014 and February 2016
210 whose tracks are shown in Figure 1. All but one monthly flight sequences consisted of four
211 individual intercontinental flights. The altitude of these flights varies typically from ~9 km
212 at the beginning of the flight to 11 - 12 km at the end before the final descent. In addition
213 to the meteorological data provided by the aircraft, meteorological parameters along the
214 flight track were calculated from the ECMWF (European Centre for Medium Range
215 Weather Forecasts) data (6-hourly, 60 model levels until February 2006 and 90 model
216 levels thereafter, $1^\circ \times 1^\circ$ horizontal resolution). Eight ~~day~~days backward, 3-D kinematic

217 trajectories were calculated with the KNMI model TRAJKS (Scheele et al., 1996,
218 http://projects.knmi.nl/campaign_support/CARIBIC/) at one minute intervals along the
219 flight path. Consequently, 5 trajectories were available for each mercury measurement. The
220 data set consists of 33 and 17 individual flights with valid TM and GEM data, respectively.

221

222 For the data evaluation, the complementary continuous meteorological and chemical data
223 were averaged over the sampling intervals of mercury measurements.

224

225 **3 Results and discussion**

226

227 3.1 Latitudinal TM distribution in the upper troposphere

228

229 Figure 2 shows latitudinal distribution of TM in the upper troposphere (defined as TM
230 concentrations at potential vorticity (PV) of $-1.5 \leq PV \leq 1.5$ PVU, $1 \text{ PVU} = 10^{-6} \text{ K m}^2 \text{ kg}^{-1} \text{ s}^{-1}$)
231 observed during the flights to South America (Bogota, São Paulo, and Rio de Janeiro)
232 in boreal summer (only July and August), fall (September, October, November), and winter
233 (December, January, February). Corresponding latitudinal distributions of acetonitrile
234 (AN), originating almost solely from biomass burning, and of CO and CH₄ with large
235 emissions from biomass burning (Andreae and Merlet, 2001) are also shown. The lowest
236 TM concentrations are observed in the latitude bands of 10 – 20°S and 20 – 30°S in summer
237 (JA) and the same applies for CO, CH₄, and acetonitrile. The highest TM concentrations in
238 20-30°S latitude band are observed in fall (SON) and the TM concentrations decrease in
239 winter (DJF) as do the CO and acetonitrile mixing ratios in the 10 – 20°S latitude band.
240 The highest CO and CH₄ mixing ratios at 20 – 30°S are observed in winter with mixing
241 ratios in fall somewhat lower. Biomass burning in South America starts in June, peaks in
242 September and ends in December (Duncan et al., 2003). TM concentrations in the
243 southernmost latitude bands follow this seasonal variability as do the acetonitrile, CO and
244 CH₄ mixing ratios at 10 – 20°S latitude. In the latitude band 20 – 30°S the CO and CH₄
245 mixing ratios are higher in boreal winter than in fall. This might result from larger
246 additional CO and CH₄ sources in boreal winter such as from oxidation of volatile organic
247 compounds and wetlands. It is also worth noting that in boreal fall and boreal winter the

248 acetonitrile and CO mixing ratios in the monitored part of the southern hemisphere are
249 higher than in the northern hemisphere. In summary, Figure 2 illustrates the large-scale
250 influence of biomass burning on the latitudinal TM distribution in the upper troposphere
251 of the southern hemisphere.

252

253 The role of biomass burning is further illustrated by means of Figure 3, comparing the
254 South America boreal winter profiles of the four trace constituents with those for South
255 Africa (Cape Town). Acetonitrile and CO mixing ratios from flights to South Africa show
256 a pronounced bulge between 30°S and 20°N peaking around the equator. The same applies
257 to results for the flights to South America, be it with somewhat lower values and more
258 southern maximum for acetonitrile. For both flight routes CO and acetonitrile mixing ratios
259 are higher in the southern than in the northern hemisphere. Boreal winter (DJF) is an
260 intermediate season between biomass emissions peaking in September in southern Africa
261 and in January in northern Africa (Duncan et al., 2003). The latitudinal pattern of CH₄ is
262 less clear, with wetlands also being a major source. Finally, Figure 3 shows a similarity
263 between TM and the biomass burning indicators in the tropics at flight altitude.

264

265 Biomass burning plumes with enhanced mercury concentrations have been reported before
266 (Brunke et al., 2001; Friedli et al., 2001, 2003a and b, Ebinghaus et al., 2007, Slemr et al.,
267 2014, among others). With 675 Mg yr⁻¹ biomass burning is estimated to be the third largest
268 source of atmospheric mercury after emissions from oceans (2682 Mg yr⁻¹) and from fossil-
269 fuel power plants (810 Mg yr⁻¹; Friedli et al., 2009; Pirrone et al., 2010). Figures 2 and 3
270 illustrate the influence of biomass burning on the large scale distribution of TM in the
271 southern hemispheric UT.

272

273 Acetonitrile mixing ratios in winter (DJF) in Figure 3 are the lowest in the northernmost
274 latitude bands 20 – 50°N. The concomitant elevated TM concentrations and CO and CH₄
275 mixing ratios are thus mostly due to anthropogenic emissions. An exception is the highest
276 TM concentration observed at 30 – 40°N (Figure 2) in summer (JA) which coincides with
277 the peak of acetonitrile mixing ratio in the northern hemisphere. The respective data
278 originate from the flight #475 from São Paulo to Munich on August 21, 2014. Two whole

279 air samples were taken within this latitude band of which sample #12 coincides with the
280 peak acetonitrile, acetone, CO, and CH₄ mixing ratios. In addition, sample #12 contains
281 high ethane and propane mixing ratios (786 and 126 ppt, respectively) as well as somewhat
282 elevated CH₄ and SF₆ mixing ratios. Sample #12 was taken over southwestern Spain and
283 its 8 [daydays](#) backward trajectory crosses the Atlantic Ocean, eastern US, Great Lakes up
284 to Californian Pacific coast. The complex composition of this sample indicates a mixture
285 of anthropogenic pollution with emissions from biomass burning. The latter is additionally
286 supported by fire maps (<https://lance.modaps.eosdis.nasa.gov/imagery/firemaps>) reporting
287 individual fire counts along the trajectory in North America and especially a large fire in
288 northern California at the time of trajectory crossing.

289

290 3.2 Seasonal variation of the vertical TM distribution in the upper troposphere and 291 lowermost stratosphere

292

293 Due to the geographical location of the airport of departure and the CARIBIC destinations
294 it happens to be that [about](#) half of the intersected air masses are above the tropopause. This
295 allows a fairly representative mapping of measured trace species around the tropopause.
296 Figure 4 shows the seasonal pattern of the average TM concentrations and CO, CH₄, and
297 O₃ mixing ratios relative to the thermal tropopause. The distance relative to the tropopause
298 is based on CARIBIC ozone measurements. Basically, an ozone mixing ratio measured by
299 CARIBIC is compared to representative data from ozone soundings. Because these
300 soundings measure both thermal tropopause height and ozone, the distance relative to the
301 tropopause is obtained (Sprung and Zahn, 2010). This value based on the CARIBIC ozone
302 data is considered to be more accurate than PV (calculated from the ECMWF-model) based
303 dynamical tropopause, especially in subtropical latitudes where the dynamical tropopause
304 is not well defined by a constant PV threshold value (Kunz et al., 2011). Only
305 measurements north of 20°N were considered for making this plot. The seasonal variation
306 of the vertical distributions of the trace gases and TM reflect their source location and the
307 Brewer-Dobson circulation with a maximum content of stratospheric air in the UT/LMS in
308 spring (Holton et al., 1995; Gettelman et al., 2014). Ozone rich air, depleted in CO, CH₄,
309 and N₂O descends in spring and the question is what happens to the mercury compounds.

310

311 The highest tropospheric TM concentrations of $1.4 - 1.7 \text{ ng m}^{-3}$ are encountered in
312 September/October at $0.5 - 1.75 \text{ km}$ below the thermal tropopause. About two thirds of
313 these elevated TM data originate from flights from Tokio to Munich on October 30, 2014,
314 and Beijing to Munich on October 31, 2014, and were observed mostly within $\sim 1500 \text{ km}$
315 of Tokio and Beijing. High TM concentrations are accompanied by elevated CO and CH₄
316 mixing ratios. Near Tokio and Beijing also elevated SF₆ mixing ratios were observed.
317 Backward trajectories from these flight segments on October 30 and 31 point to surface
318 contact in Tibet, Bangladesh, and northern India. Slightly elevated TM concentrations
319 encountered near Munich on October 30 and 31 are most likely due emissions located in
320 North America.

321

322 The lowest TM concentrations of $0.4 - 0.6 \text{ ng m}^{-3}$ were encountered during the flights
323 Tokio to Munich (CARIBIC #502) on April 21, 2015, and Mexico to Munich (CARIBIC
324 #504) on April 22, 2015. During both flights the lowest TM concentrations were
325 accompanied by O₃ and H₂O mixing ratios of $> 400 \text{ ppb}$ and $< 10 \text{ ppm}$, respectively,
326 characteristic of deeper stratospheric air. No CO data are available for the CARIBIC flight
327 #502 but CO mixing ratios of $< 30 \text{ ppb}$ for the lowest TM values during the CARIBIC
328 flight #504 also point to deep stratospheric origin of the air, as confirmed by the extremely
329 low SF₆ and CH₄ mixing ratios in both flights.

330

331 3.3 Speciation in the UT and LMS

332

333 The reason to show only TM in Figure 4, and not GEM as well is that speciation failed for
334 about half of the data due to contamination problems with the quartz wool GOM scrubber.
335 For analyzing the GEM results, we divide the data set into boreal winter (December – May)
336 and boreal summer (June – November). Figure 5 give the vertical distributions of TM and
337 GEM in three different latitude bands for boreal winter (Figure 5a) and summer (Figure
338 5b). The data points in these figures represent concentration averages and their standard
339 errors. Although extreme individual values were eliminated using the Nalimov outlier test
340 (Kaiser and Gottschalk, 1972), unedited data give very similar plots. We also note that TM

341 and GEM data from all flights were used in these figures, altogether 1528 and 1349 TM
342 measurements in winter and summer, respectively, as well 699 and 916 GEM
343 measurements in winter and summer, respectively. As already mentioned GEM data were
344 collected during the outward and TM data during the return flights. Because of different
345 flight tracks and flight altitudes the GEM and TM data cannot be directly compared even
346 if measured on the same day. In addition, because of contamination problems valid GEM
347 data are available only for about one half of the flights with TM data.

348

349 Winter vertical distribution in Figure 5a shows for 30 – 60°N a steep gradient of TM
350 concentrations across the thermal tropopause from ~ 1.25 ng m⁻³ in the UT to ~ 0.6 ng m⁻³
351 in the LMS. This gradient corresponds to the steep gradient of TM concentrations in
352 January – May shown in Figure 4. The GEM gradient is steeper starting with concentrations
353 of ~ 1.35 ng m⁻³ and decreasing to concentrations of ~ 0.35 ng m⁻³ in the LMS. The
354 difference between TM and GEM concentrations at altitudes starting at 1 km above the
355 tropopause is ~ 0.2 ng m⁻³, representing ~ 40% of TM concentration.

356

357 TM and GEM data between 30°S – 30°N cover essentially only the UT because the aircraft
358 cruising altitude of 10 – 12 km is not sufficient to enter the tropical stratosphere. TM and
359 GEM concentrations are essentially the same, but with ~1.2 ng m⁻³ somewhat lower than
360 in the UT at 30 – 60°N where most of the anthropogenic mercury sources are located.

361

362 In the northernmost latitude band (> 60°N) there are few UT data because the aircraft
363 cruising altitude of 10 – 12 km has most of the time been above the tropopause. Starting at
364 altitudes of 1 km above the tropopause, the TM concentrations around ~ 0.6 ng m⁻³ are only
365 slightly higher than GEM concentrations of 0.5 ng m⁻³. Larger difference between TM and
366 GEM concentrations is observed only at the three highest altitudes above the tropopause.

367

368 Figure 5b shows the summer data which are generally higher than the winter data. In the
369 tropical UT (30°S – 30°N) GEM concentrations are with ~ 1.2 ng m⁻³ somewhat lower than
370 those of TM, but the difference is probably insignificant. In the northern midlatitudes the
371 GEM concentrations measured in the UT are higher than TM. This is not a contradiction

372 because of the different tracks of outbound (GEM measurements) and return (TM
373 measurements) flights to North America and different influence of biomass burning on
374 particular flights. It appears that in the LMS the differences are small.

375

376 At mid latitudes and north of 60°N, TM gradients around the tropopause are much less
377 steep in summer than in winter (Figure 5a), which is consistent with the seasonal variation
378 of TM concentrations in UT/LMS shown in Figure 4. There is not much difference between
379 TM and GEM concentrations in the midlatitude LMS, but at >60°N at 2 – 3 km above the
380 tropopause GEM concentrations with ~ 0.6 ng m⁻³ are consistently lower than those of TM
381 with ~0.8 ng m⁻³.

382

383 In summary, TM concentrations are lowest (with ~ 0.5 ng m⁻³) in stratosphere at the highest
384 altitude above the tropopause (3 – 4 km). GEM concentrations are comparable to those of
385 TM in the UT, but systematically smaller in the LMS at middle latitude in winter and at
386 northernmost latitudes in summer.

387

388 Our notion about the behavior and speciation of mercury in the UT/LMS is quite limited
389 and based on a few measurement reports. Swartzendruber et al. (2006) observed at Mount
390 Bachelor higher GOM concentration in downslope air flow than in upslope flow which
391 implies higher GOM concentrations in the free troposphere than in the planetary boundary
392 layer. Talbot et al. (2007a) reported a total depletion of GEM in the UT/LMS. By
393 extrapolation of measurements in stratospheric intrusions, Lyman and Jaffe (2012) derived
394 an empirical model which predicts a total depletion of GEM at ~ 1 km above the tropopause
395 and of total mercury (including particle bound mercury, PBM) at some 2 km above the
396 tropopause. ~~The latter is inconsistent with observations of substantial PBM concentrations
397 in the stratosphere up to an altitude of 8 km above the tropopause reported by Murphy et
398 al. (1998, 2006).~~ Brooks et al. (2014) reported decreasing GOM concentrations above
399 GOM maxima at ~ 4 km altitude above ground. They also found that GEM concentrations
400 are independent of altitude between ground and 6 km altitude for most of the year. Only in
401 April, May and June GEM concentrations decreased with increasing altitude possibly
402 because of the intensive influx of stratospheric air in this season. Gratz et al. (2015)

403 observed in June 2013 high GOM concentrations in tropospheric air mass rich in BrO
404 advected from the subtropical Pacific.

405

406 Opposite to the total GEM depletion reported by Talbot et al. ~~(2007a) and predictions by~~
407 ~~Lyman and Jaffe (2012)(2007a)~~ our post-flight processed GEM and TM concentrations
408 were never below the detection limit of $\sim 0.05 \text{ ng m}^{-3}$, even at 4 km altitude above the
409 tropopause. However, when using the default Tekran software, small mercury peaks are
410 occasionally not integrated resulting in erroneous zero concentrations. We thus surmise
411 that the zero GEM concentrations reported by Talbot et al. (2007a) were not real but an
412 artifact due to incorrect default integration of the Tekran raw signal (Swartzendruber et al.,
413 2009; Slemr et al., 2016; Ambrose, 2017). We also note that Talbot et al. (2007a) attribute
414 their measurements to GEM although their inlet system is very similar to that of CARIBIC
415 (Slemr et al., 2014) with proven transmission of GOM. As for CARIBIC, the measurements
416 by Talbot et al. (2007a) are thus more likely close to those of TM.

417

418 ~~Based on TM and GEM measurements outside of a stratospheric intrusion, For the UT~~
419 Lyman and Jaffe (2012) ~~found report~~ Hg^{2+} ($\text{GOM} + \text{PBM} = \text{TM} - \text{GEM}$) ~~to be dominant~~
420 ~~mercury species at the tropopause. By extrapolation of the data using empirical correlations~~
421 ~~of TM and Hg^{2+} with ozone, they predicted zero TM concentrations already at 2 km~~
422 ~~above the tropopause and speculated that this may generally apply for the UT/LMS. This~~
423 ~~is varying between zero and $\sim 0.25 \text{ ng m}^{-3}$ at TM concentration of $\sim 1 \text{ ng m}^{-3}$. High Hg^{2+}~~
424 ~~concentrations in the UT are~~ inconsistent with our measurements ~~that~~ which show
425 comparable GEM and TM concentrations in the UT ~~with Hg^{2+} constituting at most 50%~~
426 ~~of TM up to 4 km above the tropopause. It is also inconsistent with regular. Regular~~ vertical
427 profiling of GEM, GOM, and PBM up to 6 km altitude above ground by Brooks et al.
428 (2014). ~~They report tropospheric) show~~ GOM maxima ~~of up to 0.11 ng m^{-3} at $\sim 4 \text{ km}$~~
429 above ground and decreasing GOM concentrations above. Elevated Hg^{2+} concentrations in
430 the UT during the NOMADDS (Nitrogen, Oxidants, Mercury and Aerosol Distributions,
431 Sources and Sinks) campaign were reported by Gratz et al. (2015) but only for an advected
432 tropospheric air mass with high BrO content (Gratz et al., 2015). ~~We thus conclude~~ Based
433 on this information and our own measurements it seems that high GOM concentrations in

434 the UT reported by Lyman and Jaffe (2012) ~~are most likely might be~~ an event phenomenon
435 ~~which cannot be generalized.~~

436

437 ~~Zero~~As pointed out by Lyman and Jaffe (2012), zero TM concentrations at ~ 2 km above
438 the tropopause from ~~the their~~ empirical model of Lyman and Jaffe (2012) ~~are, in addition, do~~
439 not conform to the observations of significant PBM concentrations in ~~the~~ stratosphere ~~up~~
440 ~~to 8 km above the tropopause~~ by Murphy et al. (1998, 2006). Gaseous Hg²⁺ (GOM) is
441 assumed to be in equilibrium with PBM. An extrapolation of the equilibria observed at
442 ambient air temperatures near ground (Rutter and Schauer, 2007; Amos et al., 2012) to
443 some -50°C around the tropopause ~~shows suggests~~ that almost all Hg²⁺ will be ~~on attached~~
444 ~~to~~ particles. Substantial PBM concentrations observed by Murphy et al. (1998, 2006) up to
445 8 km above the tropopause together with our TM data obtained during some 500 CARIBIC
446 flights (including those with default Tekran raw signal integration) thus exclude the
447 possibility that TM disappears at ~ 2 km above the tropopause. We also note that Murphy
448 et al. (1998, 2006) could not detect any PBM in the troposphere at and below 5 km above
449 ground. Non-detectable PBM in equilibrium with GOM at still low air temperatures at
450 these altitudes is another piece of evidence inconsistent with generally high GOM
451 concentrations in the ~~upper free troposphere~~UT.

452

453 In summary, it is plausible that our TM data currently provide the most representative
454 picture of its UT/~~LS~~LMS distribution and seasonal variation. Our GEM measurements rely
455 on the performance of the GOM quartz wool traps and the difference between TM and
456 GEM is statistically compromised by not being measured along exactly the same routes
457 and altitudes above the tropopause. Despite this, our TM and GEM observations suggest
458 only a small contribution of Hg²⁺ to TM in the UT and are consistent with the observations
459 of substantial PBM concentrations in UT/LS by Murphy et al. (1998, 2006).

460

461 3.4 Stratospheric lifetime of TM and GEM

462

463 ~~N₂O and SF₆ measured in the whole air samples taken during the CARIBIC flights can be~~
464 ~~used~~Stratospheric lifetime of a trace gas is defined as ~~chronological tracers to estimate~~

465 ~~the~~atmospheric burden of a compound divided by its stratospheric ~~lifetime of TM and~~
466 ~~GEM. Here~~sink (SPARC Report, Ko et al., eds., 2013). To determine it we use ~~here~~ the
467 relative approach described by Volk et al. (1997) ~~using~~utilizing the CARIBIC N₂O
468 measurements (Assonov et al., 2013) as reference tracer. N₂O, with a lifetime of ~120 yr
469 is nearly uniformly distributed in the troposphere, with little seasonal variation and is only
470 removed in the stratosphere (Nevison et al., 2011). In comparison with SF₆ as
471 chronological tracer, N₂O has the advantage of a much smaller latitudinal gradient in the
472 troposphere and of nearly constant growth rate in the last two decades. Figure 6 shows
473 winter (November – April) average stratospheric TM and GEM concentrations as a
474 function of N₂O mixing ratios. In this plot N₂O mixing ratios were detrended using 2015
475 as a reference year and the N₂O growth rate of 0.844 ppb yr⁻¹ (Assonov et al., 2013).

476

477 TM and GEM concentrations in Figure 6 start at 1.18 ± 0.27 (n = 48) and 1.12 ± 0.21 (n =
478 35) ng m⁻³, respectively, in the 325 – 330 ppb bin of N₂O mixing ratios and they decrease
479 substantially to 0.59 ± 0.13 (n = 12) and 0.42 ± 0.10 (n = 16) ng m⁻³, respectively, in the
480 305 – 310 ppb bin. The difference between TM and GEM concentrations is not statistically
481 significant in the 325 – 330 ppb bin of N₂O mixing ratios, i.e. in the UT as already
482 mentioned before. At lower N₂O mixing ratios, however, GEM concentrations are
483 systematically smaller than those of TM at the 99% significance level. The TM-GEM
484 difference (i.e. Hg²⁺ concentration in the gas phase (GOM) and on particles (PBM)) is
485 increasing with decreasing N₂O mixing ratios and levels off at ~0.17 ng m⁻³ at N₂O mixing
486 ratios below 315 ppb representing ~ 30% of TM concentrations. As mentioned in the
487 experimental section, the CARIBIC trace gas inlet is not optimized for quantitative
488 collection of particles and, consequently, we presume to measure only ~ 70% of Hg²⁺ on
489 particles. If all Hg²⁺ (i.e. TM-GEM) were on particles as predicted by extrapolation of Hg²⁺
490 gas-particle partitioning equilibrium (Rutter and Schauer, 2007; Amos et al., 2012) from
491 ambient temperature to temperatures at the tropopause then the unbiased Hg²⁺ and TM
492 concentrations would be ~ 0.24 and ~ 0.66 ng m⁻³, respectively, at N₂O mixing ratios below
493 310 ppb.

494

495 Small decrease of TM and GEM with decreasing N₂O below 315 ppb suggests a long
496 stratospheric lifetime of both TM and GEM. Correlations of all TM and GEM
497 concentrations at N₂O mixing ratios < 315 ppb vs N₂O yield slopes of $6.30 \pm 2.96 \text{ pg m}^{-3}$
498 ppb^{-1} (n = 46, R = 0.2947, significance > 95%) and $6.13 \pm 1.82 \text{ pg m}^{-3} \text{ ppb}^{-1}$ (n = 63, R =
499 0.3909, significance > 99%), for TM and GEM, respectively. Using stratospheric N₂O
500 lifetime of $122 \pm 24 \text{ yr}$ (Volk et al., 1997) we arrive at stratospheric TM and GEM lifetimes
501 of 72 ± 37 and $74 \pm 27 \text{ yr}$, respectively. The uncertainties calculated from the slope
502 uncertainties and the uncertainty of N₂O lifetime are probably lower limit because of the
503 narrow range of encountered N₂O mixing ratios in cruising altitudes of the CARIBIC
504 aircraft (Assonov et al., 2013). We note that our stratospheric TM and GEM lifetimes are
505 not “relatively short” as claimed by Lyman and Jaffe (2012). We think that their TM and
506 GEM concentrations were measured within the region of mixing of stratospheric with
507 tropospheric air. Figure 6 shows that TM and GEM vs N₂O correlations would result in
508 much shorter lifetimes when data at N₂O mixing ratios larger than 315 ppb were included.
509 With the calculated uncertainties the stratospheric TM lifetime cannot be distinguished
510 from that of GEM. A more precise estimate of TM and GEM stratospheric lifetimes will
511 require measurements with research aircraft capable of flying at higher altitudes.

512

513 Data in Figure 6 allow us to correlate Hg²⁺ (TM - GEM) with GEM as made by Lyman
514 and Jaffe (2012). Hg²⁺ is negatively correlated with GEM with a slope of -0.13 ± 0.04 (n =
515 7, R² = 0.712) and -0.31 ± 0.04 (n = 7, R² = 0.919) when averages and medians are used,
516 respectively. Chemical conversion of GEM into Hg²⁺ without any Hg²⁺ losses would yield
517 a slope of -1 and slopes near this value were reported for the free troposphere by
518 Swartzendruber et al. (2006) and for the UT by Lyman and Jaffe (2012). Our negative
519 slopes in the stratosphere are substantially greater than -1 and somewhat greater than -0.53
520 reported by Lyman and Jaffe (2012) for stratosphere-influenced air masses. Negative
521 slopes greater than -1 imply losses of Hg²⁺ (Hg²⁺ yield of GEM oxidation is smaller than
522 the stoichiometry of the reaction) and result in decreasing TM concentrations with
523 increasing Hg²⁺ concentrations in the stratosphere.

524

525 A reduction of TM concentration from $\sim 1.2 \text{ ng m}^{-3}$ in tropospheric air to $\sim 0.66 \text{ ng m}^{-3}$ in
526 stratospheric air is too large to be explained by the aerosol bias induced by the incomplete
527 particle sampling mentioned above and requires Hg^{2+} removal process. Such as already
528 proposed by Lyman and Jaffe (2012) such removal process requires an oxidation of GEM
529 into Hg^{2+} , an attachment of Hg^{2+} to abundant stratospheric, mainly sulfate, particles, and
530 their removal by gravitational sedimentation and/or scavenging by clouds (Menzies and
531 Tratt, 1995; Rasch et al., 2008; Lyman and Jaffe, 2012; Wilson et al., 2008). We note that
532 air mass exchange is also taking important part in removing the sulfate particles from the
533 stratosphere but TM concentrations would not change without sedimentation and
534 scavenging of Hg^{2+} on particles. The oxidation and subsequent attachment to particles
535 could be a local process in the vicinity of extratropical tropopause layer (exTL) or a non-
536 local process in the tropical upper troposphere (TTL) and during the transport from the
537 TTL to the location of the IAGOS-CARIBIC measurements in the LMS. Lyman and Jaffe
538 (2012) hypothesized that Hg^{2+} formed by GEM oxidation in the TTL and/or stratosphere
539 will attach to sulfate particles formed in the stratosphere predominantly by COS oxidation
540 and be removed with them (Wilson et al., 2008). This hypothesis is corroborated by our
541 stratospheric TM and GEM lifetimes which are comparable to COS lifetime of 64 ± 21 yr
542 (Barkley et al., 2008). As pointed out by Lyman and Jaffe (2012), the hypothetical model
543 of stratospheric mercury is thus similar and closely related to that of
544
545 If all stratospheric TM were Hg^{2+} and attached to particles then the stratospheric lifetime
546 of TM would be given by the stratospheric lifetime of particles of several years (Vaugh
547 and Hall, 2002; Friberg et al., 2018). Substantially longer TM and GEM stratospheric
548 lifetimes of ~ 70 yr suggest that the stratospheric GEM is oxidized higher up in the
549 stratosphere (Ko et al., 2013). Our TM and GEM stratospheric lifetimes are comparable to
550 COS lifetime of 64 ± 21 yr (Barkley et al., 2008) whose oxidation by photolysis and the
551 reaction with $\text{O}(^3\text{P})$ in the stratosphere is located predominantly in tropics at an altitude of
552 ~ 30 km (Brühl et al., 2012). Long stratospheric lifetimes are governed by the rate of
553 delivery of a substance to its loss region (Ko et al., 2013). Comparable stratospheric
554 lifetimes of TM, GEM, and COS thus suggest a similar location of their stratospheric loss
555 regions. At ~ 30 km altitude GEM could be oxidized by Br atoms released by the photolysis

556 [of halons and/or by reactions with O atoms \(Ko et al., 2013\). Collocation of stratospheric](#)
557 [loss regions of COS and GEM supports the hypothesis of close relation of stratospheric](#)
558 [mercury to](#) stratospheric sulfur (COS + sulfate particles) as described by Wilson et al.
559 (2008).

560

561 **Conclusions and outlook**

562

563 The obvious implication of the long stratospheric TM and GEM lifetimes is that most
564 atmospheric mercury is oxidized in the troposphere. The second direct implication is that
565 if the lifetime of GEM in the stratosphere with its very high O₃ mixing ratios (typically 1
566 ppm and more) is quite long, then the GEM + O₃ reaction cannot be important in the
567 troposphere with its low O₃ mixing ratios. This implies that either the reaction does not
568 take place or that the primary reaction product is ~~is~~-instable. Moreover, with very low
569 stratospheric H₂O mixing ratios below 10 ppm, ~~also~~-OH is [also](#) an unlikely oxidant for
570 GEM in the stratosphere. The most plausible remaining [stratospheric](#) oxidants are Br atoms
571 [originating from the decomposition of halons](#) with a possible contribution of O atoms.

572

573 The regular intercontinental IAGOS-CARIBIC flights provide an insight into the large-
574 scale distribution of TM and GEM in the UT/LMS and its seasonal variation. Post-flights
575 processed data with better accuracy and higher precision reveal a seasonal variation of
576 vertical TM distribution in the UT/LMS which is similar to most of the trace gases with
577 sources in the troposphere, such as CH₄ and CO. Importantly, even at altitudes of up to 3.5
578 km above the thermal tropopause TM concentrations are still ~0.5 ng m⁻³, one order of
579 magnitude above the instrumental detection limit. We have never observed zero TM or
580 GEM concentrations and attribute earlier reports about them to an insufficiency in the
581 default signal integration of the Tekran instrument.

582

583 Latitudinal TM distribution in the UT during the flights to South America and South Africa
584 were found to be strongly influenced by biomass burning. Although TM and GEM were
585 not measured at the same place and at the same time, the data collectively show that their
586 concentrations in the UT are similar and the Hg²⁺ concentrations are thus usually small.

587 Recent reports on high GOM and Hg²⁺ concentrations in the free troposphere are limited
588 to middle tropospheric altitudes (Brooks et al., 2014), to an event with high BrO
589 concentrations (Gratz et al., 2015) or to a stratospheric intrusion (Lyman and Jaffe, 2012)
590 and are in view of our observational IAGOS-CARIBIC data set most likely not
591 representative for large-scale UT distribution. Larger Hg²⁺ (TM – GEM) concentrations of
592 up to about half of TM concentrations were observed only in the LMS.

593

594 Lower TM concentrations were generally observed in LMS with the pronounced gradient
595 just above the tropopause. We attribute this gradient to mixing of tropospheric air with
596 stratospheric air depleted of mercury. The conservative character of TM measurements
597 implicates [thus](#) a loss process by oxidation to Hg²⁺, its attachment to particles and their
598 subsequent removal by gravitational sedimentation and/or scavenging by clouds.
599 Substantial stratospheric PBM concentrations reported by Murphy et al. (1998, 2006) and
600 GOM/PBM equilibria (Rutter and Schauer, 2007; Amos et al., 2012) extrapolated to
601 temperatures in the LMS support this hypothesis.

602

603 Correlations of TM and GEM with N₂O as a reference substance show statistically the
604 same TM and GEM concentrations in the UT. In the N₂O range of 330 and 315 ppb TM
605 and GEM concentrations rapidly decrease with decreasing N₂O mixing ratios due to mixing
606 of tropospheric air with stratospheric air depleted of mercury. Below 315 ppb until 295 ppb
607 of N₂O, TM and GEM concentrations hardly change. TM and GEM lifetimes of 72 ± 37
608 and 74 ± 27 yr, respectively, were calculated from correlations of TM and GEM vs N₂O
609 below 315 ppb, albeit with large uncertainties caused by the limited altitude range of
610 commercial airliners and the resulting narrow range of N₂O mixing ratios between 315 and
611 295 ppb. Measurements of TM, GEM, and N₂O to higher altitudes above the tropopause
612 (i.e. to N₂O mixing ratios substantially below 290 ppb) are needed to better constrain the
613 stratospheric TM and GEM lifetimes.

614

615 Stratospheric lifetimes of TM and GEM are comparable to the COS stratospheric lifetime
616 of 64 ± 21 yr (Barkley et al., 2008), which is in volcanically quiet periods the major
617 precursor of sulfate particles in the stratosphere (Wilson et al., 2008). [Comparable COS](#)

618 [and GEM stratospheric lifetimes suggest collocation of their loss regions](#). This coincidence
619 corroborates the hypothesis of Hg²⁺ attachment to sulfate particles and their removal by
620 gravitational sedimentation and scavenging by clouds. This hypothesis, first proposed by
621 Lyman and Jaffe (2012), could be directly tested in future by quantitative measurements of
622 Hg/S ratios on stratospheric particles. Such measurements would also better constrain the
623 mercury fluxes across the tropopause.

624

625 Mercury measurements onboard IAGOS-CARIBIC were stopped in March 2016 and the
626 space of the mercury instrument is now occupied by other instruments. The reason for the
627 termination of the mercury measurements was the feeling that, with the present
628 instrumentation, we will only reproduce the existing data. An improved instrumentation
629 including reliable speciation technique is needed to gain new insights. Any institution
630 capable of providing and maintaining such an instrument is welcomed to participate in
631 future IAGOS-CARIBIC measurements. For details please consult the CARIBIC
632 coordinator Andreas Zahn.

633

634 **Acknowledgements**

635

636 We thank Lufthansa Airlines and Lufthansa Technik for their commitment and support.

637 We also thank Jan Boedewadt from HZG for modifying the Tekran instrument for
638 deployment in the CARIBIC container. The development and operation of the CARIBIC
639 system has been financially supported by the German Ministry of Education and Science
640 (AFO 2000, IAGOS-D), by the European Commission's DGXII Environment RTD 4th
641 and 5th Framework programs, by grants from the Max Planck Society and from Frankfurt
642 Airport.

643

644 **References**

645

646 AMAP/UNEP: Technical Background Report for the Global Mercury Assessment, 2013,
647 available at AMAP (www.amap.no) and UNEP Chemicals Branch's
648 (<http://www.unep.org/hazardoussubstances/mercury/informationmaterials/reportsandpublications/tabid/3593/default.aspx>) websites.

650

651 Ambrose, J.L., Lyman, S.N., Huang, J., Gustin, M.S., and Jaffe, D.A.: Fast time resolution
652 oxidized mercury measurements during the Reno Atmospheric Mercury Intercomparison
653 Experiment (RAMIX), *Environ. Sci. Technol.*, 47, 7285-7294, 2013.

654

655 ~~Ambrose, J.L.~~, Gratz, L.E., Jaffe, D.A., Campos, T., Flocke, F.M., Knapp, D.J., Stechman,
656 D.M., Stell, M., Weinheimer, A.J., Cantrell, C.A., and Mauldin III, R.L.: Mercury emission
657 ratios from coal-fired power plants in the southeastern United States during NOMADDS,
658 *Environ. Sci. Technol.*, 49, 10389-10397, 2015.

659

660 Ambrose, J.L.: Improved methods for signal processing in measurements of Hg^0 by
661 Tekran 2537A and 2537B instruments, *Atmos. Meas. Tech.*, 10, 5063-5073, 2017.

662

663 Amos, H.M., Jacob, D.J., Holmes, C.D., Fisher, J.A., Wang, Q., Yantosca, R.M, Corbitt,
664 E.S., Galarneau, E., Rutter, A.P., Gustin, M.S., Steffen, A., Schauer, J.J., Graydon, J.A.,
665 Louis, V.L.St., Talbot, R.W., Edgerton, E.S., Zhang, Y., and Sunderland, E.M.: Gas-
666 particle partitioning of atmospheric Hg(II) and its effect on global mercury deposition,
667 *Atmos. Chem. Phys.*, 12, 591-603, 2012.

668

669 Andreae, M.O., and Merlet, P.: Emission of trace gases and aerosols from biomass burning,
670 *Global Biogeochem. Cycles*, 15, 955-966, 2001.

671

672 Ariya, P.A., Amyot, M., Dastoor, A., Deeds, D., Feinberg, A., Kos, G., Poulain, A.,
673 Ryjkov, A., Semeniuk, K., Subir, M., and Toyota, K.: Mercury physicochemical and

674 biogeochemical transformation in the atmosphere and at atmospheric interfaces: A review
675 and future direction, *Chem. Rev.*, 115, 3760-3802, 2015.

676

677 Assonov, S.S., Brenninkmeijer, C.A.M., Schuck, T., and Umezawa, T.: N₂O as a tracer of
678 mixing stratospheric and tropospheric air based on CARIBIC data with applications for
679 CO₂, *Atmos. Environ.*, 79, 769-779, 2013.

680

681 Banic, C.M., Beauchamp, S.T., Tordon, R.J., Schroeder, W.H., Steffen, A., Anlauf, K.A.,
682 and Wong, K.H.T.: Vertical distribution of gaseous elemental mercury in Canada, *J.*
683 *Geophys. Res.*, 108 (D9), 4264, doi:10.1029/2002JD002116, 2003.

684

685 Barkley, M.P., Palmer, P.I., Boone, C.D., Bernath, P.F., and Sunthralanigam, P.: Global
686 distributions of carbonyl sulfide in the upper troposphere and stratosphere, *Geophys. Res.*
687 *Lett.*, 35, L14810, doi:10.1029/2008GL034270, 2008.

688

689 Baron, P. A., and Willeke K.: *Aerosol Measurements: Principles, Techniques and*
690 *Applications*, John Wiley and Sons, New York, 1131 pp, 2001.

691

692 Bieser, J., Slemr, F., Ambrose, J., Brenninkmeijer, C., Brooks, S., Dastoor, A., DeSimone,
693 F., Ebinghaus, R., Gencarelli, C.N., Geyer, B., Gratz, L.E., Hedgecock, I.M., Jaffe, D.,
694 Kelley, P., Lin, C.-J., Jaegle, L., Matthias, V., Ryjkov, A., Selin, N.E., Song, S., Travnikov,
695 O., Weigelt, A., Luke, W., Ren, X., Zahn, A., Yang, X., Zhu, Y., and Pirrone, N.: Multi-
696 model study of mercury dispersion in the atmosphere: vertical and interhemispheric
697 distribution of mercury species, *Atmos. Chem. Phys.*, 17, 6925-6955, 2017.

698

699 Brenninkmeijer, C.A.M., Crutzen, P., Boumard, F., Dauer, T., Dix, B., Ebinghaus, R.,
700 Filippi, D., Fischer, H., Franke, H., Friß, U., Heintzenberg, J., Helleis, F., Hermann, M.,
701 Kock, H.H., Koeppel, C., Lelieveld, J., Leuenberger, M., Martinsson, B.G., Miemczyk, S.,
702 Moret, H.P., Nguyen, H.N., Nyfeler, P., Oram, D., O'Sullivan, D., Penkett, S., Platt, U.,
703 Pupek, M., Ramonet, M., Randa, B., Reichelt, M., Rhee, T.S., Rohwer, J., Rosenfeld, K.,
704 Scharffe, D., Schlager, H., Schumann, U., Slemr, F., Sprung, D., Stock, P., Thaler, R.,

705 Valentino, F., van Velthoven, P., Waibel, A., Wandel, A., Waschitschek, K., Wiedensohler,
706 A., Xueref-Remy, I., Zahn, A., Zech, U., and Ziereis, H.: Civil aircraft for the regular
707 investigation of the atmosphere based on an instrumented container: The new CARIBIC
708 system, *Atmos. Chem. Phys.*, 7, 1-24, 2007.
709
710 Brooks, S., Ren, X., Cohen, M., Luke, W.T., Kelley, P., Artz, R., Hynes, A., Landing, W.,
711 and Martos, B.: Airborne vertical profiling of mercury speciation near Tullahoma, TN,
712 USA, *Atmosphere*, 5, 557-574, 2014.
713
714 [Brühl, C., Lelieveld, J., Crutzen, P.J., and Tost, H.: The role of carbonyl sulfide as a source](#)
715 [of stratospheric sulfate aerosol and its impact on climate, *Atmos. Chem. Phys.*, 12, 1239-](#)
716 [1253, 2012.](#)
717
718 Brunke, E.-G., Labuschagne, C., and Slemr, F.: Gaseous mercury emissions from a fire in
719 the Cape Peninsula, South Africa, during January 2000, *Geophys. Res. Lett.*, 28, 1483-
720 1486, 2001.
721
722 Dibble, T.S., Zelic, M.J., and Mao, H.: Thermodynamics of reactions of ClHg and BrHg
723 radicals with atmospherically abundant free radicals, *Atmos. Chem. Phys.*, 12, 10271-
724 10279, 2012.
725
726 Duncan, B.R., Martin, R.V., Staudt, A.C., Yevich, R., and Logan, J.A.: Interannual and
727 seasonal variability of biomass burning emissions constrained by satellite observations, *J.*
728 *Geophys. Res.*, 108, doi: 10.1029/2002JD002378, 2003.
729
730 Ebinghaus, R. and Slemr, F.: Aircraft measurements of atmospheric mercury over southern
731 and eastern Germany, *Atmos. Environ.*, 34, 895-903, 2000.
732
733 Ebinghaus, R., Slemr, F., Brenninkmeijer, C.A.M., van Velthoven, P., Zahn, A., Hermann,
734 M., O'Sullivan, D.A., and Oram, D.E.: Emissions of gaseous mercury from biomass

735 burning in South America in 2005 observed during CARIBIC flights, *Geophys. Res. Lett.*,
736 34, L08813, doi:10.1029/2006GL028866, 2007.

737

738 [Friberg, J., Martinsson, B.G., Andersson, S.M., and Sandvik, O.S.: Volcanic impact on the](#)
739 [climate – the stratospheric aerosol load in the period 2006 – 2015, *Atmos. Chem. Phys.*](#)
740 [Discuss., doi:10.5194/acp-2017-1200.](#)

741

742 Friedli, H.R., Radke, L.F., and Yu, J.Y.: Mercury in smoke from biomass fires, *Geophys.*
743 *Res. Lett.*, 28, 3223-3226, 2001.

744

745 Friedli, H.R., Radke, L.F., Lu, J.Y., Banic, C.M., Leaitch, W.R., and MacPherson, J.I.:
746 Mercury emissions from burning of biomass from temperate North American forests:
747 laboratory and airborne measurements, *Atmos. Environ.*, 37, 253-267, 2003a.

748

749 Friedli, H.R., Radke, L.F., Prescott, R., Hobbs, P.V., and Sinha, P.: Mercury emissions
750 from the August 2001 wildfires in Washington State and an agricultural waste fire in
751 Oregon and atmospheric mercury budget estimates, *Global Biogeochem. Cycles*, 17,
752 doi:10.1029/2002GB001972, 2003b.

753

754 Friedli, H.R., Radke, L.F., Prescott, R., Li, P., Wo, J.-H., and Carmichael, G.R.: Mercury
755 in the atmosphere around Japan, Korea, and China as observed during the 2001 ACE-Asia
756 field campaign: Measurements, distributions, sources, and implications, *J. Geophys. Res.*,
757 109, D19S25, doi:10.1029/2003JD004244, 2004.

758

759 Friedli, H.R., Arellano, A.F., Cinnirella, S., and Pirrone, N.: Initial estimates of mercury
760 emissions to the atmosphere from global biomass burning, *Environ. Sci. Technol.*, 43,
761 3507-3513, 2009.

762

763 Gettelman, A., Hoor, P., Pan, L.L., Randel, W.J., Hegglin, M.I., and Birner, T.: The
764 extratropical upper troposphere and lower stratosphere, *Rev. Geophys.*, 49, RG3003,
765 doi:10.1029/2011RG000355, 2011.

766

767 Gratz, L.E., Ambrose, J.L., Jaffe, D.A., Shah, V. Jaeglé, L., Stutz, J., Festa, J., Spolaor, M.,
768 Tsai, C., Selin, N.E., Song, S., Zhou, X., Weinheimer, A.J., Knapp, D.J., Montzka, D.D.,
769 Flocke, F.M., Campos, T.L., Apel, E., Hornbrook, R., Blake, N.J., Hall, S., Tyndall, G.S.,
770 Reeves, M., Stechman, D., and Stell, M.: Oxidation of mercury by bromine in the
771 subtropical Pacific free troposphere, *Geophys. Res. Lett.*, 42, doi:10.1002/2015GL066645,
772 2015.

773

774 Gustin, M.S., Amos, H.M., Huang, J., Miller, M.B., and Heidecorn, K.: Measuring and
775 modeling mercury in the atmosphere: a critical review, *Atmos. Chem. Phys.*, 15, 5697-
776 5713, 2015.

777

778 Holmes, C.D., Jacob, D.J., Corbitt, E.S., Mao, J., Yang, X., Talbot, R., and Slemr, F.:
779 Global atmospheric model for mercury including oxidation by bromine atoms, *Atmos.*
780 *Chem. Phys.*, 10, 12037-12057, 2010.

781

782 Holton, J.R., Haynes, P.H., McIntyre, M.E., Douglass, A.R., Rood, R.B., and Pfister, L.:
783 Stratosphere-troposphere exchange, *Rev. Geophys.*, 33, 403-439, 1995.

784

785 Horowitz, H.M., Jacob, D.J., Zhang, Y., Dibble, T.S., Slemr, F., Amos, H.M., Schmidt,
786 J.A., Corbitt, E.S., Marais, E.A., and Sunderland, E.M.: A new mechanism for atmospheric
787 mercury redox chemistry: Implications for the global mercury budget, *Atmos. Chem.*
788 *Phys.*, 17, 6353-6371, 2017.

789

790 Kaiser, R., and Gottschalk, G.: Elementare Tests ~~zur~~ Beurteilung von Meßdaten,
791 Bibliographisches Institut, Mannheim, 1972.

792

793 [Ko, M.K.W., Newman, P.A., Reimann, S., and Strahan, S.E., eds.: Lifetimes of](#)
794 [stratospheric ozone-depleting substances, their replacements, and related species, SPARC](#)
795 [Report No. 6. WCRP-15/2013, December 2013.](#)

796

Formatiert: Englisch (Vereinigte Staaten)

797 Kunz, A., Konopka, P., Müller, R., and Pan, L.L.: Dynamical tropopause based on
798 isentropic potential vorticity gradients, *J. Geophys. Res.*, 116, D01110,
799 doi:10.1029/2010JD014343, 2011.
800

801 Lin, C.-J., Pongprueksa, P., Lindberg, S.E., Pehkonen, S.O., Byun, D., and Jang, C.:
802 Scientific uncertainties in atmospheric mercury models. I. Model science evaluation,
803 *Atmos. Environ*, 40, 2911-2928, 2006.
804

805 Lindberg, S., Bullock, R., Ebinghaus, R., Engstrom, D., Feng, X., Fitzgerald, W., Pirrone,
806 N., Prestbo, E., and Seigneur, C.: A synthesis of progress and uncertainties in attribution
807 the sources of mercury in deposition, *Ambio*, 36, 19-32, 2007.
808

809 Lyman, S.N., and Jaffe, D.A.: Formation and fate of oxidized mercury in the upper
810 troposphere and lower stratosphere, *Nature Geosci.*, 5, 114-117, 2012.
811

812 Menzies, R.T., and Tratt, D.M.: Evidence of seasonally dependent stratosphere-
813 troposphere exchange and purging of lower stratospheric aerosol from a multiyear lidar
814 data set, *J. Geophys. Res.*, 100, D2, 3139-3148, 1995.
815

816 Mergler, D., Anderson, H.A., Chan, L.H.M., Mahaffey, K.R., Murray, M., Sakamoto, M.,
817 and Stern, A.H.: Methyl mercury exposure and health effects in humans: A worldwide
818 concern, *Ambio*, 36, 3-11, 2007.
819

820 Murphy, D.M., Thomson, D.S., and Mahoney, M.J.: In situ measurements of organics,
821 meteoritic material, mercury, and other elements in aerosols at 5 to 19 kilometers, *Science*,
822 282, 1664-1669, 1998.
823

824 Murphy, D.M., Hudson, P.K., Thomson, D.S., Sheridan, P.J., and Wilson, J.C.:
825 Observations of mercury-containing aerosols, *Environ. Sci. Technol.*, 40, 3163-3167,
826 2006.
827

828 Nevison, C.D., Dlugokencky, E., Dutton, G., Elkins, J.W., Fraser, P., Hall, B., Krummel,
829 P.B., Langenfelds, R.L., O'Doherty, S., Prinn, R.G., Steele, L.P., and Weiss, R.F.:
830 Exploring causes of interannual variability in the seasonal cycles of tropospheric nitrous
831 oxide, *Atmos. Chem. Phys.*, 11, 3713-3730, 2011.
832
833 Pirrone, N., Cinnirella, S., Feng, X., Finkelman, R.B., Friedli, H.R., Leaner, J., Mason, R.,
834 Mukherjee, A.B., Stracher, G.B., Streets, D.G., and Telmer, K.: Global mercury emissions
835 to the atmosphere from anthropogenic and natural sources, *Atmos. Chem. Phys.*, 10, 5951-
836 5964, 2010.
837
838 Radke, L.F., Friedli, H.R., and Heikes, B.G.: Atmospheric mercury over the NE Pacific
839 during spring 2002: Gradients, residence time, upper troposphere lower stratosphere loss,
840 and long-range transport, *J. Geophys. Res.*, 112, D19305, doi:10.1029/2005JD005828,
841 2007.
842
843 Rasch, P.J., Tilmes, S., Turco, R.P., Robock, A., Oman, L., Chen, C.-C., Stenchikov, G.L.,
844 and Garcia, R.R.: An overview of geoengineering of climate using stratospheric sulphate
845 aerosols, *Phil. Trans. R. Soc. A*, 366, 4007-4037, 2008.
846
847 Rutter, A.P., and Schauer, J.J.: The effect of temperature on the gas-particle partitioning of
848 reactive mercury in atmospheric aerosols, *Atmos. Environ.*, 41, 8647-8657, 2007.
849
850 Scheele, M., Siegmund, P., and Van Velthoven, P.: Sensitivity of trajectories to data
851 resolution and its dependence on the starting point: In or outside a tropopause fold,
852 *Meteorol. Appl.*, 3, 267-273, 1996.
853
854 Scheuhammer, A.M., Meyer, M.W., Sandheinrich, M.B., and Murray, M.W.: Effects of
855 environmental methylmercury on the health of wild bird, mammals, and fish, *Ambio*, 36,
856 12-18, 2007.
857

858 Selin, N.E., Jacob, D.J., Park, R.J., Yantosca, R.M., Strode, S., Jaeglé, L., and Jaffe, D.:
859 Chemical cycling and deposition of atmospheric mercury: Global constraints from
860 observations, *J. Geophys. Res.*, 112, D02308, doi:10.1029/2006JD007450, 2007.
861

862 Slemr, F., Ebinghaus, R., Brenninkmeijer, C.A.M., Hermann, M., Kock, H.H., Martinsson,
863 B.G., Schuck, T., Sprung, D., van Velthoven, P., Zahn, A., and Ziereis, H.: Gaseous
864 mercury distribution in the upper troposphere and lower stratosphere observed onboard the
865 CARIBIC passenger aircraft, *Atmos. Chem. Phys.*, 9, 1957-1969, 2009.
866

867 Slemr, F., Weigelt, A., Ebinghaus, R., Brenninkmeijer, C., Baker, A., Schuck, T., Rauthe-
868 Schöch, A., Riede, H., Leedham, E., Hermann, M., van Velthoven, P., Oram, D.,
869 O'Sullivan, D., Dyroff, C., Zahn, A., and Ziereis, H.: Mercury plumes in the global upper
870 troposphere observed during flights with the CARIBIC observatory from May 2005 until
871 June 2013, *Atmosphere* 5, 342-369, 2014.
872

873 Slemr, F., Weigelt, A., Ebinghaus, R., Kock, H.H., Bödewadt, J., Brenninkmeijer, C.A.M.,
874 Rauthe-Schöch, A., Weber, S., Hermann, M., Becker, J., Zahn, A., and Martinsson, B.:
875 Atmospheric mercury measurements onboard the CARIBIC passenger aircraft, *Atmos.*
876 *Meas. Tech.*, 9, 2291-2302, 2016.
877

878 [Sprovieri, F., Pirrone, N., Ebinghaus, R., Kock, H., and Dommergue, A: A review of](#)
879 [worldwide atmospheric mercury measurements. *Atmos. Chem. Phys.*, 10, 8245-8265,](#)
880 [2010.](#)
881

882 Sprung, D., and Zahn, A.: Acetone in the upper troposphere/lowermost stratosphere
883 measured by the CARIBIC passenger aircraft: Distribution, seasonal cycle, and variability,
884 *J. Geophys. Res.*, 115, D16301, doi:10.1029/2009JD012099, 2010.
885

886 Swartzendruber, P.C., Jaffe, D.A., Prestbo, E.M., Weiss-Penzias, P., Selin, N.E., Park, R.,
887 Jacob, D.J., Strode, S., and Jaeglé, L.: Observations of reactive gaseous mercury in the free

888 troposphere at the Mount Bachelor Observatory, *J. Geophys. Res.*, 111, D24301,
889 doi:10.1029/2006JD007415, 2006.
890
891 Swartzendruber, P.C., Chand, D., Jaffe, D.A., Smith, J., Reidmiller, D., Gratz, L., Keeler,
892 J., Strode, S., Jaeglé, L., and Talbot, R.: Vertical distribution of mercury, CO, ozone, and
893 aerosol scattering coefficient in the Pacific Northwest during the spring 2006 INTEX-B
894 campaign, *J. Geophys. Res.*, 113, D10305, doi:10.1029/2007JD009579, 2008.
895
896 Swartzendruber, P.C., Jaffe, D.A., and Finley, B.: Improved fluorescence peak integration
897 in the Tekran 2537 for applications with sub-optimal sample loadings, *Atmos. Environ.*,
898 43, 3648-3651, 2009.
899
900 Talbot, R., Mao, H., Scheuer, E., Dibb, J., and Avery, M.: Total depletion of Hg⁰ in the
901 upper troposphere – lower stratosphere, *Geophys. Res. Lett.*, 34, L23804,
902 doi:10.1029/2007GL031366, 2007a.
903
904 Talbot, R., Mao, H., Scheuer, E., Dibb, J., Avery, M., Browell, E., Sachse, G., Vay, S.,
905 Blake, D., Huey, G., and Fuelberg, H.: Factors influencing the large-scale distribution of
906 Hg⁰ in the Mexico City area and over the North Pacific, *Atmos. Chem. Phys. Discuss.*, 7,
907 15533-15563, 2007b.
908
909 Travnikov, O., Angot, H., Artaxo, P., Bencardino, M., Bieser, J., D'Amore, F., Dastoor,
910 A., De Simone, F., Carmen Diéguez, M., Dommergue, A., Ebinghaus, R., Feng, X.B.,
911 Gencarelli, C.N., Hedgecock, I.M., Magand, O., Martin, L., Matthias, V., Mashyanov, N.,
912 Pirrone, N., Ramachandran, R., Read, K.A., Ryjkov, A., Selin, N.E., Sena, F., Song, S.,
913 Sprovieri, F., Wip, D., Wängberg, I., and Yang, X.: Multi-model study of mercury
914 dispersion in the atmosphere: atmospheric processes and model evaluation, *Atmos. Chem.*
915 *Phys.*, 17, 5271-5295, 2017.
916

917 Volk, C.M., Elkins, J.W., Fahey, D.W., Dutton, G.S., Gilligan, J.M., Loewenstein, M.,
918 Podolske, J.R., Chan, K.R., and Gunson, M.R.: Evaluation of source gas lifetimes from
919 stratospheric observations, J. Geophys. Res. 102, D21, 25543-25564, 1997.

920 [▲](#)
921 [Waugh, D.W., and Hall, T.M.: Age of stratospheric air: Theory, observations, and models,](#)
922 [Rev. Geophys. 40, doi:10.1029/2000RG000101, 2002.](#)

923
924 Weigelt, A., Ebinghaus, R., Pirrone, N., Bieser, J., Bödewadt, J., Esposito, G., Slemr, F.,
925 van Velthoven, P.F.J., Zahn, A., and Ziereis, H.: Tropospheric mercury vertical profiles
926 between 500 and 10000 m in central Europe, Atmos. Chem. Phys., 16, 4135-4146, 2016a.

927
928 Weigelt, A., Slemr, F., Ebinghaus, R., Pirrone, N., Bieser, J., Bödewadt, J., Esposito, G.,
929 and van Velthoven, P.F.J.: Mercury emissions of a coal-fired power plant in Germany,
930 Atmos. Chem. Phys., 16, 13653-13668, 2016b.

931
932 Wilson, J.C., Lee, S.-H., Reeves, J.M., Brock, C.A., Jonsson, H.H., Lafleur, B.G.,
933 Loewenstein, M., Podolske, J., Atlas, E., Boehring, K., Toon, G., Fahey, D., Bui, T.P.,
934 Diskin, G., and Moore, F.: Steady-state aerosol distributions in the extra-tropical, lower
935 stratosphere and the processes that maintain them, Atmos. Chem. Phys., 8, 6617-6626,
936 2008.

937 [▲](#)
938

Formatiert: Schriftart: 12 Pt., Englisch (Vereinigte Staaten)

Formatiert: Standard (Web), Links, Tabstopps: 14,75 cm,
Links + 16 cm, Links

Formatiert: Schriftart: Fett

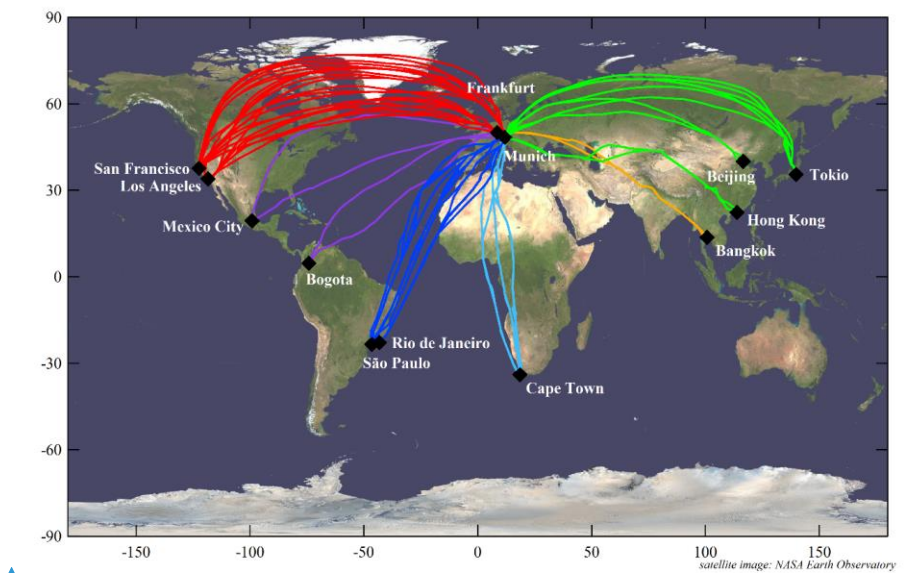
Formatiert: Links

939 **Figures**

940

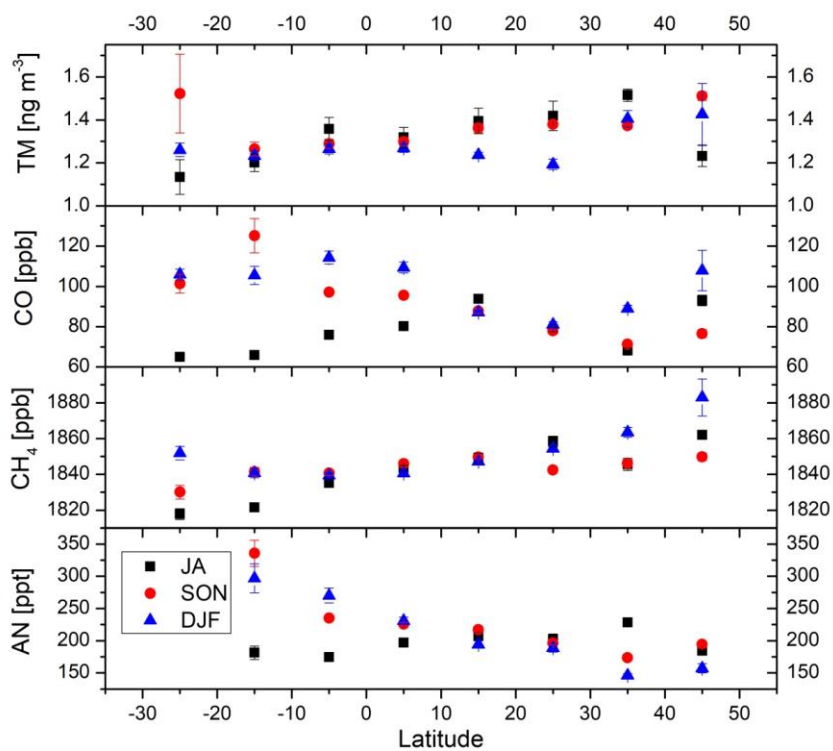
941 Figure 1: Tracks of the CARIBIC flights made between April 2014 and February 2016
942 (CARIBIC flights #468-536). Mercury data for these flights were obtained by post-flight
943 processing of the Tekran raw signal (Slemr et al., 2016).

944



Formatiert: Englisch (Vereinigte Staaten)

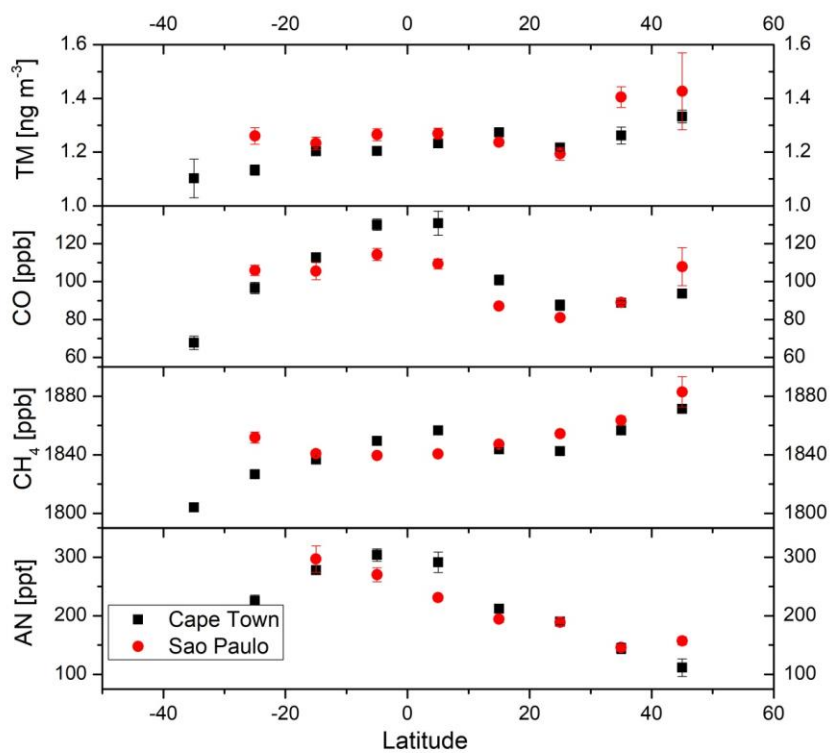
948 Figure 2: Latitudinal distributions of tropospheric ($PV \leq 1.5$ PVU) TM, CO, CH₄, and
949 acetonitrile (AN) during the flights from Bogota and São Paulo/Rio de Janeiro to Munich
950 in summer (only July and August, JA), autumn (September, October, and November, SON)
951 and winter (December, January, and February, DJF). The points represent averages and the
952 vertical bars their standard error. No acetonitrile data were available south of 20°S.
953



Formatiert: Englisch (Vereinigte Staaten)

954
955
956

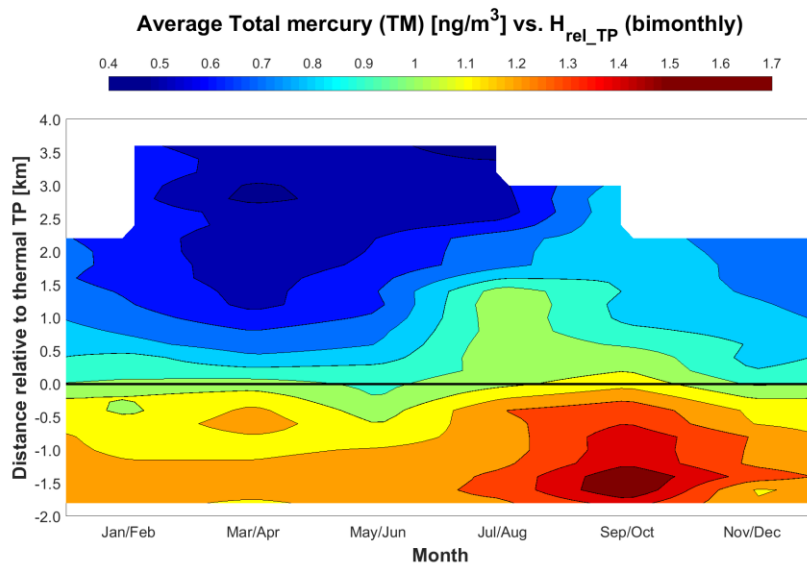
957 Figure 3: Latitudinal distributions of tropospheric TM, CO, CH₄, and acetonitrile (AN) in
958 winter (December, January, and February, DJF) during the flights from Cape Town and
959 São Paulo to Munich. The points represent averages and the vertical bars their standard
960 error. No acetonitrile data are available south of 30°S and 20°S for flights to Cape Town
961 and São Paulo, respectively.
962



Formatiert: Englisch (Vereinigte Staaten)

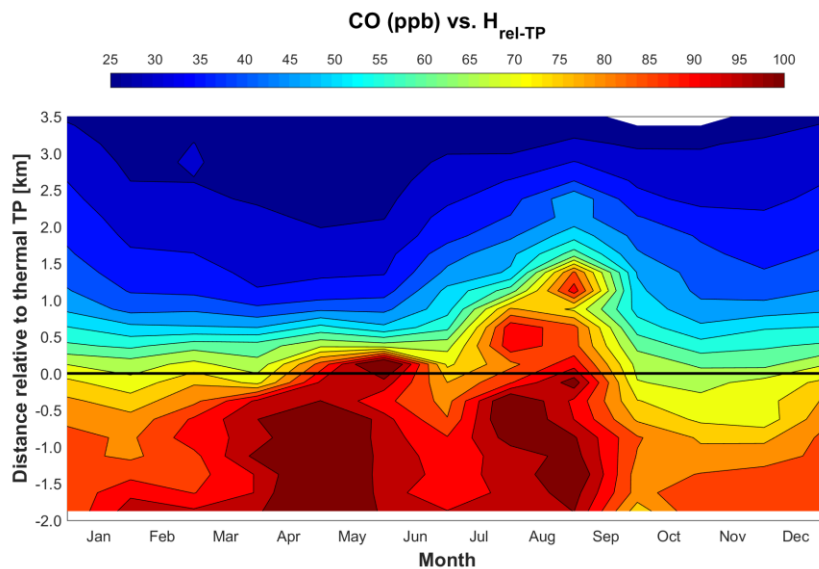
963
964

965 Figure 4: Seasonal variation of mean TM concentrations (a), CO (b), CH₄ (c) and O₃ (d)
966 mixing ratios in distance relative to the thermal tropopause derived from ozone soundings
967 according to Sprung and Zahn (2010). All TM data north of 20°N obtained between April
968 2014 and February 2016 were considered for this plot (2288 individual data points).
969



Formatiert: Englisch (Vereinigte Staaten)

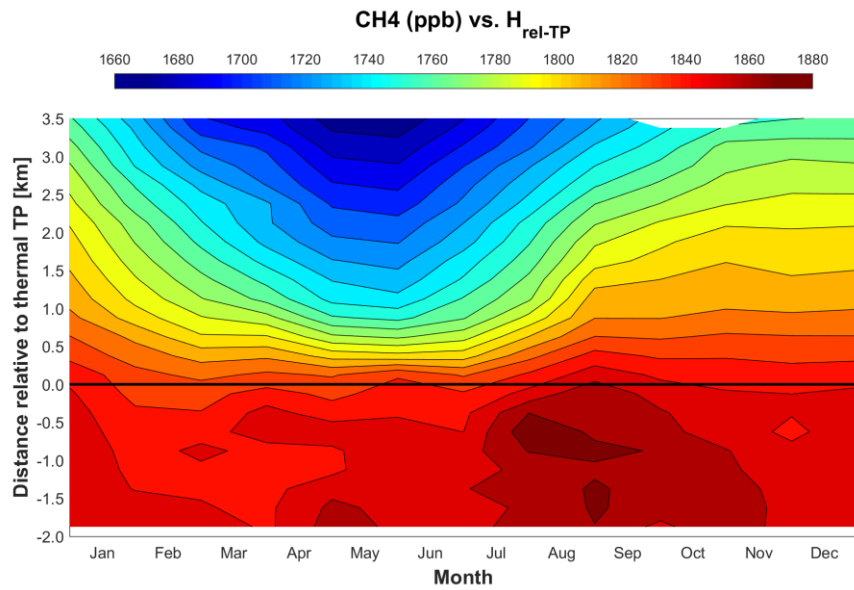
970
971



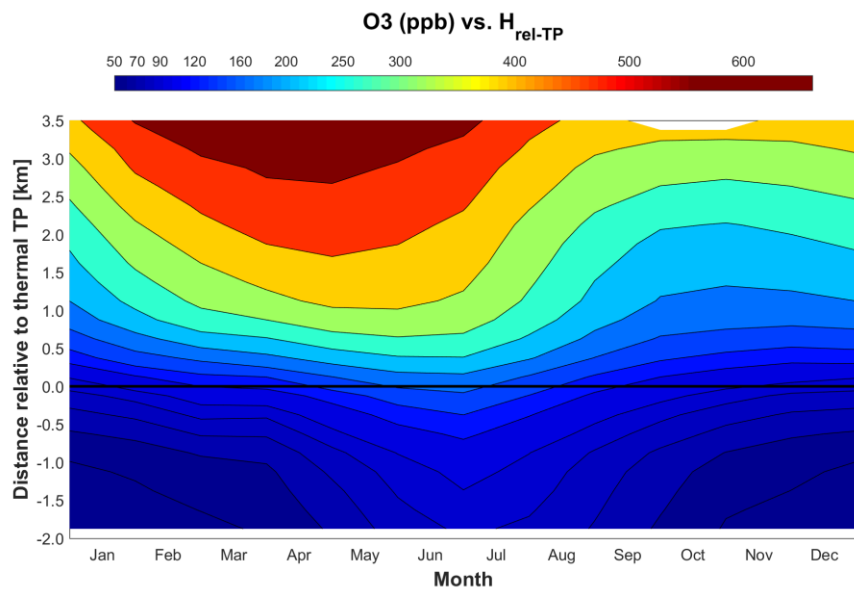
Formatiert: Englisch (Vereinigte Staaten)

972

Formatiert: Englisch (Vereinigte Staaten)



Formatiert: Englisch (Vereinigte Staaten)

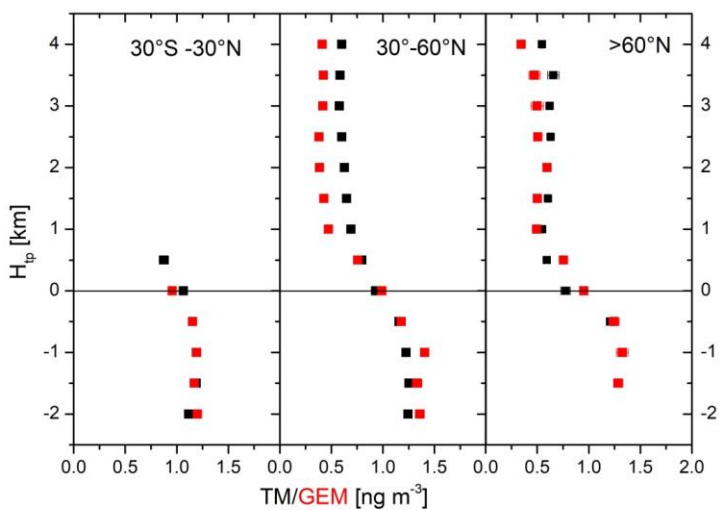


Formatiert: Englisch (Vereinigte Staaten)

973
974

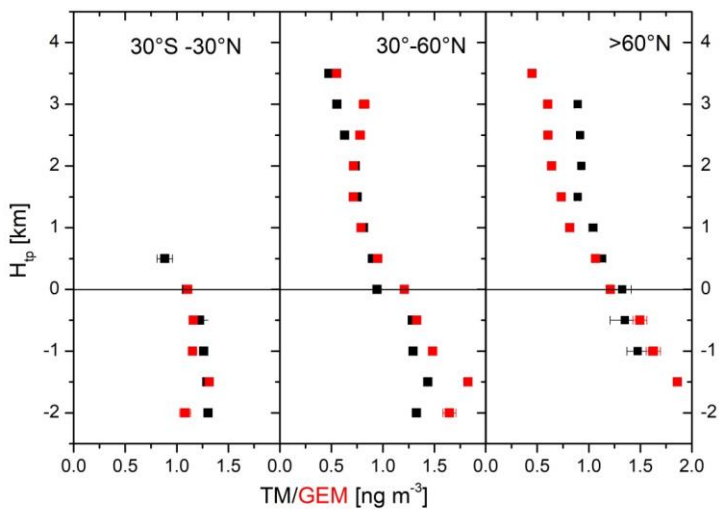
975

976 Figure 5: Vertical TM and GEM distribution relative to the thermal tropopause in a)
 977 winter (December – May, upper panel) and b) in summer (June – November, lower
 978 panel). The data points represent averages and their standard errors, extreme values were
 979 eliminated using the Nalimov outlier test (Kaiser and Gottschalk, 1972).
 980



Formatiert: Englisch (Vereinigte Staaten)

981

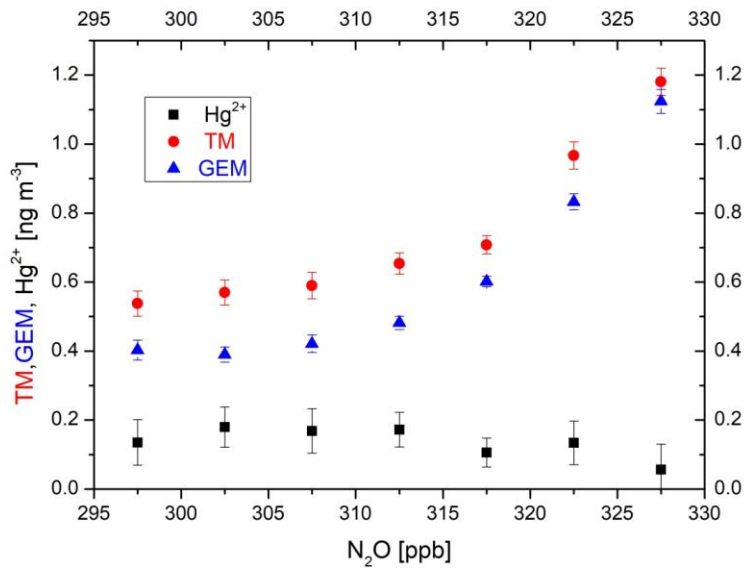


Formatiert: Englisch (Vereinigte Staaten)

982
983

984
985
986
987
988
989

Figure 6: Stratospheric average TM and GEM concentrations in boreal winter (November – April) are binned according to the N₂O mixing ratio. N₂O mixing ratios were detrended using 2015 as a reference year and the N₂O growth rate of 0.844 ppb yr⁻¹ (Assonov et al., 2013). Vertical and horizontal bars represent the standard errors of the averages.



Formatiert: Englisch (Vereinigte Staaten)

990